Applied Catalysis B: Environmental 160–161 (2014) 552–557

Contents lists available at ScienceDirect

Applied Catalysis B: Environmental

journal homepage: www.elsevier.com/locate/apcatb

Rapid microwave-assisted syntheses of reduced graphene oxide (RGO)/$ZnIn_2S_4$ microspheres as superior noble-metal-free photocatalyst for hydrogen evolutions under visible light

Lin Ye, Zhaohui Li*

Research Institute of Photocatalysis, State Key Laboratory of Photocatalysis on Energy and Environment, College of Chemistry, Fuzhou University, 523# Gongye Road, Fuzhou 350002, PR China

ARTICLE INFO

Article history:
Received 24 March 2014
Received in revised form 30 May 2014
Accepted 8 June 2014
Available online 13 June 2014

Keywords:
$ZnIn_2S_4$
RGO
Microwave
Photocatalytic
Hydrogen evolution

ABSTRACT

A rapid microwave-assisted method has been developed for the preparations of flower-like RGO/$ZnIn_2S_4$ microspheres which are consisted of interwoven nanosheets of $ZnIn_2S_4$ and RGO. The as-prepared samples were characterized by X-ray diffraction (XRD), Fourier transform infrared spectroscopy (FT-IR), Raman spectroscopy, X-ray photoelectron spectroscopy (XPS), scanning electron microscopy (SEM), transmission electron microscopy (TEM) and high-resolution transmission electron microscopy (HRTEM). The mechanism for the formation of the flower-like microspheres of RGO/$ZnIn_2S_4$ nanocomposites via the microwave-assisted method has been proposed. As compared with the samples obtained solvothermally, the RGO/$ZnIn_2S_4$ microspheres obtained via the microwave-assisted method show highly enhanced photocatalytic performance for hydrogen evolution under visible light irradiations, due to the existence of strong interaction between $ZnIn_2S_4$ and RGO. The highest hydrogen evolution rate (132.3 $\mu mol\ h^{-1}$), observed over an optimum RGO loading amount of 1.0 wt%, is comparable to that over 1.0 wt%-Pt/$ZnIn_2S_4$ (129.0 $\mu mol\ h^{-1}$). This work demonstrates the important role played by microwave heating in the preparations of RGO-based materials. The results also highlight the potential of using RGO as a non-noble metal cocatalyst in the photocatlaytic hydrogen evolution process.

1. Introduction

Hydrogen production from photocatalytic water-splitting provides a potential opportunity to obtain clean, renewable and storable energy from abundant water using solar energy [1–3]. Since the discovery of the photocatalytic splitting of water on TiO_2 by Fujishima and Honda, the technology of using semiconductor-based photocatalysts for hydrogen production has been attracting a lot of attention [4]. So far, a variety of active photocatalysts, including metal oxides [5–7], sulfides [8–10], oxynitrides [11,12], as well as the metal-free semiconductors have already been developed for hydrogen production [13].

Among all the already reported photocatalysts, metal sulfides are regarded as good candidates for photocatalytic hydrogen production due to their strong absorption in the visible light region. Ternary $ZnIn_2S_4$, a semiconductor chalcogenide with suitable band gap (2.34–2.48 eV), was previously reported to exhibit two distinct polymorphs based on cubic and hexagonal lattices which can be controlled synthesized via a facile hydrothermal method using different precursors [14,15]. Previous studies revealed that both polymorphs of $ZnIn_2S_4$ are active for photocatalytic hydrogen production under visible light irradiations [14,16–18]. However, the hydrogen-production rate over pure $ZnIn_2S_4$ is still limited. Numerous attempts, such as doping transition-metal ions like Cu, incorporation of multi-walled carbon nanotubes (MWCNTs), RGO, polymers and metal chalcogenides, have been tried to improve the photocatalytic performance of $ZnIn_2S_4$-based photocatalytic systems [8,9,19–23]. Especially, the incorporation of RGO into $ZnIn_2S_4$ has been found to influence the hydrogen evolution performance of $ZnIn_2S_4$ [24]. Highly reductive RGO/$ZnIn_2S_4$ nanocomposites show significantly enhanced photocatalytic activity for hydrogen evolution not only because RGO can serve as an excellent electron acceptor to restrict the recombination of the photo-generated charge carriers, but also it can act as the mediator for the transportation of the photogenerated electrons as well as the co-catalyst for hydrogen evolution. However, the already reported routes to RGO/$ZnIn_2S_4$ nanocomposites are restricted to either hydrothermal or solvothermal method which requires a relatively long reaction time.

* Corresponding author. Tel.: +86 591 83779260; fax: +86 591 83779260.
E-mail addresses: zhaohuili1969@yahoo.com, zhaohuili@fzu.edu.cn (Z. Li).

http://dx.doi.org/10.1016/j.apcatb.2014.06.012
0926-3373/

Microwave-assisted synthesis is a highly efficient technology in the preparations of nanomaterials since usually products with small particle size, narrow size distribution and high purity can be obtained from the microwave-assisted process in a short reaction time [25,26]. In particular, microwave-assisted irradiation has been utilized to obtain ultrathin RGO nanosheets with only a few layer of graphene since microwave irradiation can help to exfoliate GO [27–29]. Although microwave-assisted method has already been reported for the preparations of a few of RGO-semiconductor nanocomposites like RGO/ZnO and RGO/CdS, it has never been applied in the synthesis of RGO/$ZnIn_2S_4$ nanocomposites [30,31].

Herein, we reported a rapid microwave-assisted method in the preparations of RGO/$ZnIn_2S_4$ nanocomposites. Unlike product obtained via a normal solvothermal method which shows two-dimensional flake morphology, the microwave-assisted method gave flower-like RGO/$ZnIn_2S_4$ microspheres which are consisted of interwoven nanosheets of $ZnIn_2S_4$ and ultrathin RGO [23]. As compared with the product obtained solvothermally, the RGO/$ZnIn_2S_4$ microspheres obtained via the microwave-assisted method show highly enhanced photocatalytic performance for hydrogen evolution under visible light irradiations, due to the existence of the strong interaction between $ZnIn_2S_4$ and RGO.

2. Experimental

2.1. Preparations

All the reagents are analytical grade and used without further purifications. Graphene oxide (GO) was synthesized following the Hummers' method with a slight modification. For the synthesis of RGO/$ZnIn_2S_4$, different amount of GO were dispersed in a mixed solution containing 30 ml *N*,*N*-dimethylformamide (DMF) and 30 ml ethylene glycol (EG) followed by ultrasonication for 60 min. Then $ZnCl_2$ (0.136 g, 1 mmol) and $InCl_3{\cdot}4H_2O$ (0.586 g, 2 mmol) was added to the GO dispersion and the suspension continue to ultrasonicate for a few minutes. After that, thioacetamide (TAA) (0.3 g, 4 mmol) was added into the mixture under vigorous stirring. The resultant suspension was sealed in a Teflon-lined double-walled digestion vessel. After treating the solution at a controllable temperature of 200 °C for 90 min using a microwave system (Ethos A, Milestone, Italy), the vessel was then cooled to room temperature. The product was collected by centrifugation, washed with deionized water and absolute ethanol, and dried at 60 °C. The RGO/$ZnIn_2S_4$ nanocomposites with different amount of RGO are denoted as *x* wt%-RGO/$ZnIn_2S_4$. Pure $ZnIn_2S_4$ was synthesized similarly without the addition of GO.

2.2. Characterizations

Powder X-ray diffraction (XRD) were collected using a Bruker D8 Advance X-ray diffractometer (Cu *K*α irradiations). Raman spectroscopy was performed using an invia-Reflex Micro-Raman Spectroscopy system (Renishaw Co.) with 532 nm line of an Ar ion laser at room temperature. The IR analyses were carried out on a Nicolet 670 FT-IR spectrometer. The morphology of the samples was obtained by a field emission scanning electron microscopy (SEM) (JSM-6700F). The transmission electron microscopy (TEM) and high resolution transmission electron microscopy (HRTEM) images were obtained in a JEOL model JEM 2010 EX instrument at an accelerating voltage of 200 kV. The powder particles were supported on a carbon film coated on a 3 mm diameter fine-mesh copper grid. The sample suspension in ethanol was sonicated and a drop was dripped on the support film. X-ray photoelectron spectroscopy (XPS) measurements were performed on a PHI Quantum 2000 XPS system (PHI, USA) with a monochromatic Al *K*α source and a charge neutralizer. All the binding energy is reference to C 1s peak observed in the XPS spectrum of pure $ZnIn_2S_4$. BET surface area was carried out on an ASAP2020M apparatus (Micromeritics Instrument Corp., USA). For BET surface area analyses, the samples were degassed in vacuum at 200 °C for 10 h and then measured at 77 K. UV–vis diffuse reflectance spectra (UV-DRS) of the powders were obtained for the dry-pressed disk samples using a Cary 500 Scan Spectrophotometer (Varian, USA). $BaSO_4$ was used as a reflectance standard in the UV–vis diffuse reflectance experiment. Electrochemical impedance spectroscopy (EIS) were measured on an electrochemical analyzer (Zahner, Germany) in a standard three-electrode system using the prepared samples as the working electrodes with an active area of ca. 0.25 cm^2, a Pt wire as the counter electrode, and Ag/AgCl (saturated KCl) as a reference electrode. Na_2SO_4 (0.2 M) aqueous solution was used as the electrolyte. Impedance data were fitted with ZSimpWin software (Princeton Applied Research). A 300 W Xe arc lamp equipped with a 420 nm cutoff filter served as a light source. Photoluminescence (PL) spectra were carried out on a fluorescence spectrometer (Hitachi F-4500). The PL emission spectra of pure $ZnIn_2S_4$ and RGO/$ZnIn_2S_4$ with different amount of RGO were obtained, respectively, with a 260 nm wavelength as the excitation source.

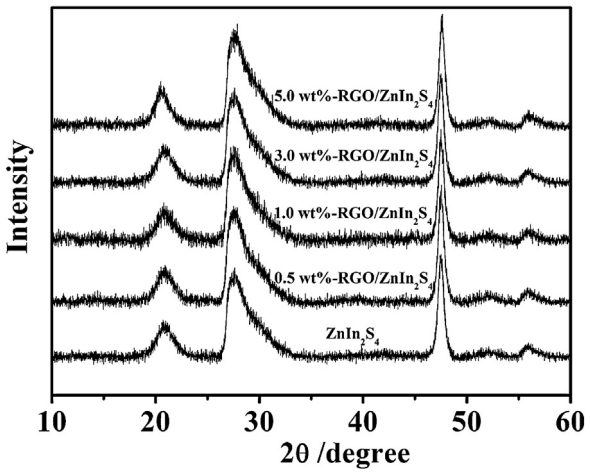

Fig. 1. XRD patterns of pure $ZnIn_2S_4$ and RGO/$ZnIn_2S_4$ nanocomposites with different amount of RGO.

2.3. Photocatalytic hydrogen evolution

Photocatalytic experiments for hydrogen evolution were carried out in a closed gas circulation and evacuation system fitted with a top Pyrex window. 50 mg of photocatalyst was dispersed in 100 ml of aqueous solution containing 2.0 ml lactic acid as sacrificial reagents. The suspension was irradiated with a 300 W Xe lamp equipped with a 420 nm cut-off filter to provide the visible light irradiations. The temperature of the reactant solution was maintained at room temperature by a flow of cooling water during the photocatalytic reaction. The amount of hydrogen evolved was determined with an on-line gas chromatograph equipped with a TCD detector.

3. Results and discussion

The RGO/$ZnIn_2S_4$ nanocomposites were synthesized by reacting $ZnCl_2$, $InCl_3$ and TAA in a mixed solvent of DMF and EG in the presence of different amount of GO via a microwave-assisted method. Fig. 1 shows the XRD patterns of the as-obtained samples. The XRD pattern of the sample obtained in absence of GO can be indexed to pure hexagonal $ZnIn_2S_4$ (JCPDS-03-065-2023).

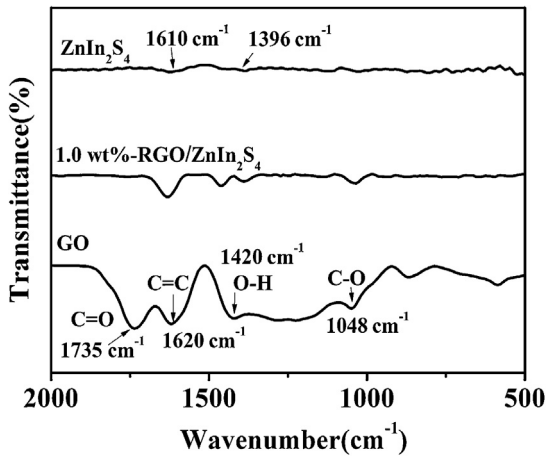

Fig. 2. FTIR spectra of GO, $ZnIn_2S_4$ and 1.0 wt%-RGO/$ZnIn_2S_4$ nanocomposites.

All the samples obtained in the presence of different amount of GO show characteristic XRD patterns as the pure hexagonal $ZnIn_2S_4$, indicating that the presence of GO in the reaction mixture does not influence the formation of hexagonal $ZnIn_2S_4$. No diffractions peaks corresponding to either GO or RGO has been observed in the XRD patterns of the resultant products, probably due to its low amount and relatively low diffraction intensity. However, the existence of RGO in the nanocomposite can be confirmed by the FT-IR and Raman spectra. The FT-IR spectra of pristine $ZnIn_2S_4$ show only two small peaks at 1610 cm^{-1} and 1396 cm^{-1} in the region of 2000–500 cm^{-1}, corresponding to the surface absorbed water molecules and the hydroxyl groups [32] (Fig. 2). On the contrary, RGO/$ZnIn_2S_4$ nanocomposites show peaks at 1048 cm^{-1}, 1450 cm^{-1} and 1620 cm^{-1} corresponding to the C—O stretching vibrations, O—H deformation vibrations and skeletal vibration of graphene, respectively, The peak at 1735 cm^{-1} which assigned to C=O vibration observed on GO totally disappears in the RGO/$ZnIn_2S_4$ nanocomposites, while that at 1048 cm^{-1} significant decreases, indicating that GO has been successfully reduced to RGO during the microwave process [23,30]. The Raman spectra of RGO/$ZnIn_2S_4$ nanocomposites show peaks at 1346 cm^{-1} and 1596 cm^{-1}, corresponding to the D band and G band of RGO (Fig. 3). The ratio of I_D/I_G over the nanocomposites is determined to be ca. 1.20, much higher than that observed over the original GO (0.91). Since the ratio of I_D/I_G is an indicator of the graphitization degree

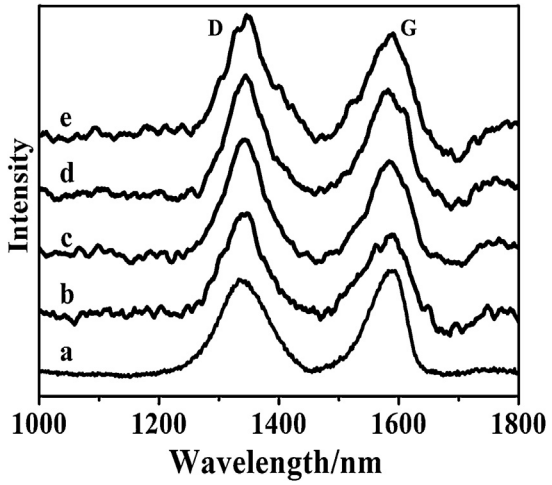

Fig. 3. Raman spectra of (a) GO; (b) 0.5 wt%-RGO/$ZnIn_2S_4$; (c) 1.0 wt%-RGO/$ZnIn_2S_4$; (d) 3.0 wt%-RGO/$ZnIn_2S_4$; (e) 5.0 wt%-RGO/$ZnIn_2S_4$ nanocomposites.

of carbonaceous materials, the higher I_D/I_G observed over the as-prepared nanocomposites as compared to that of GO suggests a successful reduction of GO to RGO in the nanocomposites [33]. These results confirmed that GO was reduced to RGO and a successful incorporation of RGO in the resultant nanocomposites.

XPS analyses were carried out to study the surface chemical composition and electronic state of 1.0 wt%-RGO/$ZnIn_2S_4$ nanocomposites and the results were shown in Fig. 4. The XPS spectrum of 1.0 wt%-RGO/$ZnIn_2S_4$ nanocomposites in the C 1s region show peaks at 284.8 eV and 286.6 eV, which are assigned to sp^2-hybridized carbon (C—C) and epoxy/hydroxyl carbon (C—O) [34,35] (Fig. 4a). As compared to original GO, the intensity of the peak ascribed to the epoxy/hydroxyls carbon (C—O) (286.8 eV) in the nanocomposite significantly decreases, while the peak corresponding to the carboxyl (C=O) (288.5 eV) totally disappears, in consistent with the FT-IR result (Fig. S1). As shown in Fig. 4b–d, characteristic binding energy of 1045.5 eV for Zn^{2+} $2p_{1/2}$ and 1022.3 eV for Zn^{2+} $2p_{3/2}$, 445.0 eV for In^{3+} $3d_{5/2}$ and 452.6 eV for In^{3+} $3d_{3/2}$, 161.5 eV for S^{2-} $2p_{3/2}$ and 162.8 eV for S^{2-} $2p_{1/2}$ are observed in the XPS spectra of 1.0 wt%-RGO/$ZnIn_2S_4$ nanocomposites. As compared with pure $ZnIn_2S_4$, the binding energy for 1.0 wt%-RGO/$ZnIn_2S_4$ nanocomposites shift slightly, suggesting the existence of the electronic interaction between the incorporated RGO and $ZnIn_2S_4$ in the nanocomposites [23,36].

The morphology of the as-synthesized RGO/$ZnIn_2S_4$ nanocomposites was studied by SEM and TEM. Flower-like microspheres in a dimension of about 300–350 nm are observed in the SEM image of a typical 1.0 wt%-RGO/$ZnIn_2S_4$ nanocomposite (Fig. 5a) The microsphere morphology observed over the microwave-assisted synthesized sample is quite different from the two dimensional sheet-on-sheet flake-like RGO/$ZnIn_2S_4$ nanocomposites prepared via a normal solvothermal method which we reported previously [23]. This indicates that the microwave heating process plays an important role for the formation of the flower-like microspheres. The TEM image of the 1.0 wt%-RGO/$ZnIn_2S_4$ nanocomposite clearly shows that the flower-like microspheres are consisted of large numbers of interwoven ultrathin nanosheets (Fig. 5b). Clear lattice-fringe spacing of 0.32 nm can be assigned to the (1 0 2) crystal plane of hexagonal phase of $ZnIn_2S_4$, indicating the formation of well-defined crystal structure of hexagonal $ZnIn_2S_4$ in the microspheres. Moreover, the lattice-fringe corresponding to hexagonal $ZnIn_2S_4$ interweave with amorphous RGO area, indicating there exists intimate contact between hexagonal $ZnIn_2S_4$ and RGO nanosheets (Fig. 5c).

According to our previous study on the two-dimensional flake-like RGO/$ZnIn_2S_4$ nanocomposites obtained via a normal solvothermal process, the hydrophilic functional groups (e.g. —OH, —COOH) on GO surface can act as the active sites for the adsorption of Zn^{2+} and In^{3+} cations [23,37]. These surface adsorbed cations can further react with S^{2-} anions decomposed from TAA to form $ZnIn_2S_4$ nuclei on the surface, followed by an anisotropic growth to give $ZnIn_2S_4$ nanosheets due to the intrinsic lamellar structure of hexagonal $ZnIn_2S_4$ phase. In the meantime, GO is reduced to RGO by the organic solvent and a final sheet-on-sheet two-dimensional flake-like RGO/$ZnIn_2S_4$ nanocomposites were obtained due to a less RGO exfoliation degree. However, no large dimension of RGO nanosheets were observed in the current product obtained from the microwave-assisted method. We believed that this phenomenon may be ascribed to a higher RGO exfoliation degree which leads to easily curling up ultrathin RGO layers. Actually previous studies on the preparations of RGO-based materials have also revealed that microwave heating can help to exfoliate GO and lead to thinner RGO nanosheets [27–29,38]. Without a thick enough RGO nanosheet as the support, the as-formed $ZnIn_2S_4$ nanosheets and the curled RGO nanosheets can assemble together to form the flowerlike microspheres as what we have previously reported on the hydrothermal

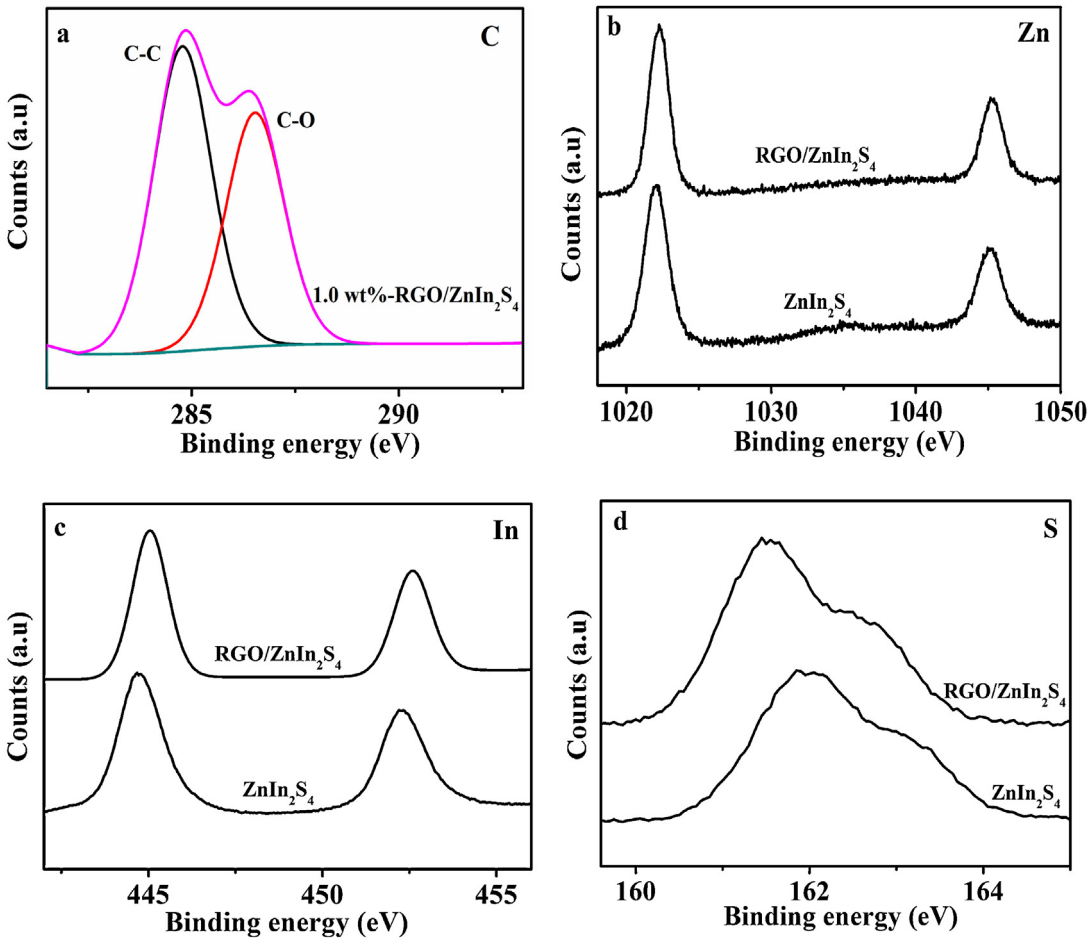

Fig. 4. XPS spectra in C 1s region for (a) 1.0 wt%-RGO/$ZnIn_2S_4$ nanocomposites; XPS spectra of (b) Zn^{2+} 2p; (c) In^{3+} 3d; (d) S^{2-} 2p in pure $ZnIn_2S_4$ and 1.0 wt%-RGO/$ZnIn_2S_4$ nanocomposites.

formation of $ZnIn_2S_4$ microspheres [24]. However, as compared to the normal heating process, the microwave-assisted heating is more efficient, which lead to faster nucleation and anisotropic growth of $ZnIn_2S_4$. Therefore, the dimension of the as-obtained RGO/$ZnIn_2S_4$ microspheres is much smaller than those obtained hydrothermally [14].

The UV–vis diffuse reflectance spectra of RGO/$ZnIn_2S_4$ nanocomposites with different amount of RGO were shown in Fig. 6. Similar with the RGO/$ZnIn_2S_4$ prepared by solvothermal method, the incorporation of RGO into $ZnIn_2S_4$ does not obviously change the band gap of $ZnIn_2S_4$, but an enhanced absorbance in the visible-light region with increasing RGO content is observed. This is in agreement with the color change of the RGO/$ZnIn_2S_4$ nanocomposites from yellow to dark green with the increasing RGO amount [39].

The photocatalytic performance for hydrogen evolution over the as-obtained RGO/$ZnIn_2S_4$ nanocomposites was carried out under visible light irradiations using lactic acid as the sacrificial agent. Fig. 7 shows the rate for photocatalytic hydrogen evolution over pure $ZnIn_2S_4$ and RGO/$ZnIn_2S_4$ loaded with different amounts of RGO. The introduction of only 0.5 wt% RGO can significantly increase the hydrogen evolution rate to 108.1 $\mu mol\ h^{-1}$, an almost 8.2 times as that over pure $ZnIn_2S_4$ (13.2 $\mu mol\ h^{-1}$). An optimum RGO loading amount is found at 1.0 wt%, which exhibits the highest photocatalytic performance with a hydrogen evolution rate of 132.3 $\mu mol\ h^{-1}$. This rate is comparable to that observed over 1.0 wt% Pt loaded $ZnIn_2S_4$ (129.0 $\mu mol\ h^{-1}$), indicating that RGO can be a promising non-noble metal cheap co-catalyst for $ZnIn_2S_4$ [8]. When the amount of incorportated RGO exceeds 1.0 wt%, the photocatalytic hydrogen evolution rate over RGO/$ZnIn_2S_4$

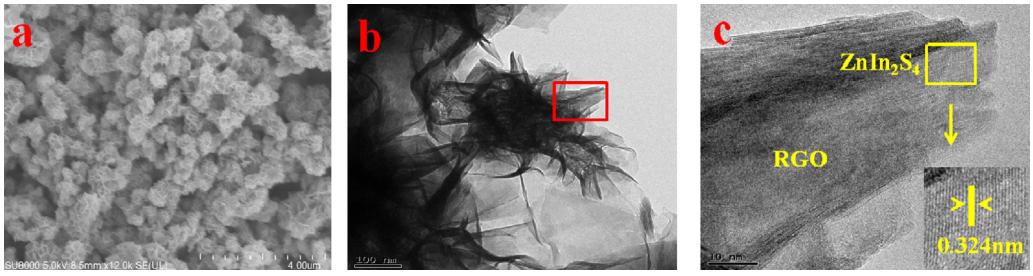

Fig. 5. The morphology of 1.0 wt%-RGO/$ZnIn_2S_4$ nanocomposites (a) SEM image; (b) low magnification TEM image; (c) HRTEM image.

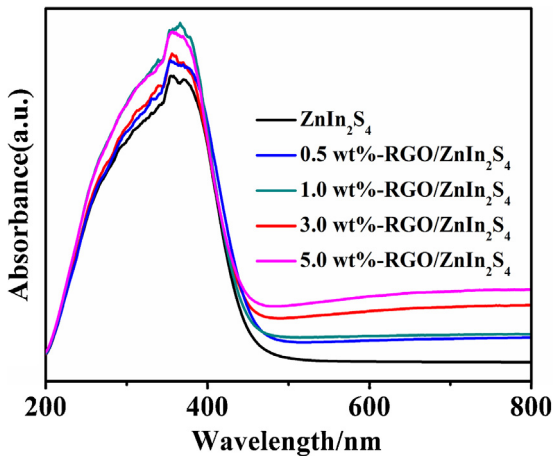

Fig. 6. UV–vis DRS spectra of pure $ZnIn_2S_4$ and RGO/$ZnIn_2S_4$ nanocomposites with different amount of RGO. (For interpretation of the references to color in this figure legend, the reader is referred to the web version of this article.)

nanocomposites decreases. A decrease of the photocatalytic activity with the increase of the RGO amount has previously been observed over some RGO-semiconductor nanocomposites and is ascribed to the shielding effect of RGO [40–42]. Therefore, similar to other RGO/semiconductor nanocomposites, an appropriate RGO loading amount is required to achieve the optimized photocatalytic activity.

As compared with RGO/$ZnIn_2S_4$ prepared by a normal solvothermal method, the hydrogen evolution rate over the microwave-assisted synthesized product enhanced significantly. The optimum hydrogen evolution rate (132.3 $\mu mol\,h^{-1}$) over RGO/$ZnIn_2S_4$ nanocomposites prepared by microwave-assisted method is about 3.3 times as that over solvothermally prepared RGO/$ZnIn_2S_4$ nanocomposites (40.7 $\mu mol\,h^{-1}$) under otherwise similar reaction condition (Fig. S2). Since both samples show similar light absorption in the visible light region and comparable BET specific area (157.2 $m^2\,g^{-1}$ for microwave-assisted prepared sample, while 150.0 $m^2\,g^{-1}$ for solvothermally obtained one), their different photocatalytic activity can not be explained in terms of these factors (Fig. 8).

Our previous study on the photocatalytic performance of the solvothermal prepared sheet-on-sheet RGO/$ZnIn_2S_4$ nanocomposites revealed that the enhanced performance over the nanocomposites can be ascribed to an electron transfer from the CB of $ZnIn_2S_4$ to RGO which results in an effective hole–electron separation. The high electronic conductivity of the nanocomposites can facilitate the transportation of the electron to the

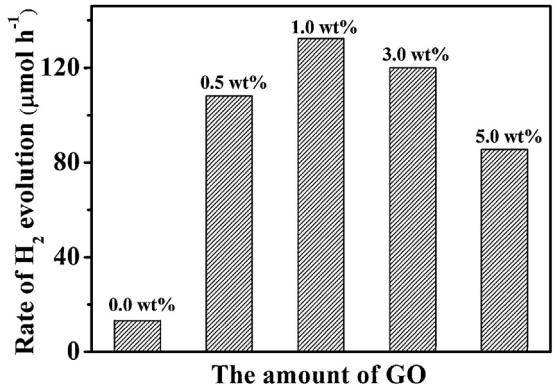

Fig. 7. Hydrogen evolution rate over pure $ZnIn_2S_4$ and RGO/$ZnIn_2S_4$ with different RGO loading amount.

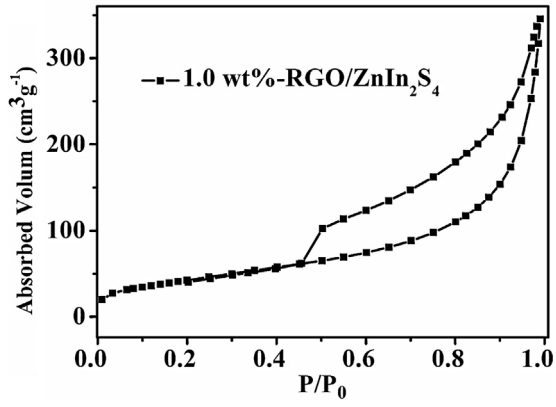

Fig. 8. Nitrogen adsorption–desorption isotherms of 1.0 wt%-RGO/$ZnIn_2S_4$ nanocomposites.

defective carbon sites in RGO, which act as active hydrogen evolution sites to reduce H_2O. The effectiveness of the electron transfer from $ZnIn_2S_4$ to RGO is influenced by the interaction between $ZnIn_2S_4$ and RGO in the nanocomposites, while the transportation is determined by the electronic conductivity of the nanocomposites [42,43]. Since the product obtained via the microwave-assisted method is flower-like microspheres consisted of interwoven nanosheets of $ZnIn_2S_4$ and RGO, the interaction between these two components should be stronger as compared to that in the sheet-on-sheet two dimensional flake-like RGO/$ZnIn_2S_4$ nanocomposites obtained via a normal solvothermal reaction. Moreover, the flowerlike RGO/$ZnIn_2S_4$ microspheres also show a higher conductivity. As shown in Fig. 9, the electrochemical impedance spectra (EIS) analysis reveals that the microwave-assisted prepared 1.0 wt%-RGO/$ZnIn_2S_4$ nanocomposites shows a smaller semicircle as compared with that of the flake-like RGO/$ZnIn_2S_4$ nanocomposites prepared solvothermally, suggesting its superior electronic conductivity which would facilitate the electron transportation in RGO. Since photoluminescence (PL) technique is a generally utilized method to investigate the recombination rate of the photo-generated charger carriers, the PL spectra of the 1.0 wt%-RGO/$ZnIn_2S_4$ nanocomposites has also been investigated [44]. It was found that the intensity of the PL peak of the microwave-assisted prepared RGO/$ZnIn_2S_4$

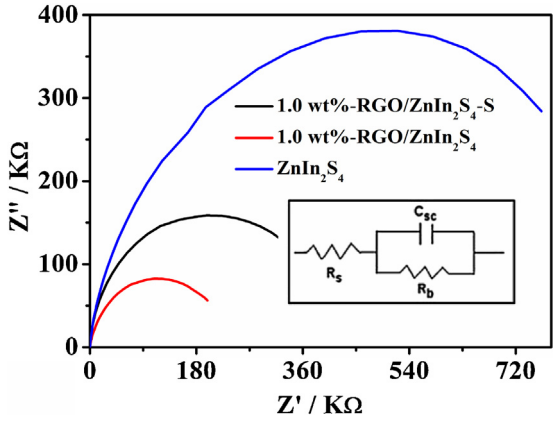

Fig. 9. Nyquist plots of experimental impedance data for pure $ZnIn_2S_4$, microwave-assisted prepared 1.0 wt%-RGO/$ZnIn_2S_4$ and 1.0 wt%-RGO/$ZnIn_2S_4$ prepared by solvothermal method, in the frequency range of 0.01 Hz to 1.0×10^5 Hz using an ac bias of 0 V vs. Ag/AgCl without visible light irradiations in 0.2 M Na_2SO_4 aqueous solution. (Inset: Electrical equivalent circuit used for fitting of impedance spectra. R_s, C_{sc} and R_b represent electrolyte resistance, space charge capacitance and bulk electrode resistance, respectively.)

microspheres decreases as compared to that of pure $ZnIn_2S_4$, and is lower than that prepared solvothermally, in agreement with its higher photocatalytic activity (Fig. S3). This result demonstrates that as compared with the normal solvothermal process, the microwave-assisted method is a more superior method in the preparations of RGO/$ZnIn_2S_4$ nanocomposites for application in photocatalysis.

4. Conclusion

In summary, a rapid microwave-assisted method has been developed for the preparations of flower-like RGO/$ZnIn_2S_4$ microspheres which are consisted of interwoven nanosheets of $ZnIn_2S_4$ and RGO. The strong interaction between RGO and $ZnIn_2S_4$ makes the as-obtained RGO/$ZnIn_2S_4$ microspheres to show highly enhanced photocatalytic performance for hydrogen evolution under visible light irradiations as compared to samples obtained solvothermally. The highest photocatalytic hydrogen evolution rate, observed over an optimum RGO loading amount of 1.0 wt%, is comparable to that over 1.0 wt%-Pt/$ZnIn_2S_4$. This work demonstrates the important role played by microwave in the preparations of RGO-based materials. The results also highlight the potential of using RGO as a non-noble metal cocatalyst in the photocatlaytic hydrogen evolution.

Acknowledgments

The work was supported by NSFC (21273035), 973 Programs (2014CB239303) and Specialized Research Fund for the Doctoral Program of Higher Education (20123514110002). Z. Li thanks the Award Program for Minjiang Scholar Professorship for financial support.

Appendix A. Supplementary data

Supplementary data associated with this article can be found, in the online version, at http://dx.doi.org/10.1016/j.apcatb.2014.06.012.

References

[1] N.S. Lewis, D.G. Nocera, Proc. Nat. Acad. Sci. U.S.A. 103 (2006) 15729–15735.
[2] H. Tong, S.X. Ouyang, Y.P. Bi, N. Umezawa, M. Oshikiri, J.H. Ye, Adv. Mater. 24 (2012) 229–251.
[3] X.B. Chen, S.H. Shen, L.J. Guo, S.S. Mao, Chem. Rev. 110 (2010) 6503–6570.
[4] A. Fujishima, K. Honda, Nature 238 (1972) 37–38.
[5] W.J. Ren, Z.H. Ai, F.L. Jia, L.Z. Zhang, X.X. Fan, Z.G. Zou, Appl. Catal., B: Environ. 69 (2007) 138–144.
[6] F. Zuo, K. Bozhilov, R.J. Dillon, L. Wang, P. Smith, X. Zhao, C. Bardeen, P.Y. Feng, Angew. Chem. Int. Ed. 51 (2012) 6223–6226.
[7] M. Altomare, M. Pozzi, M. Allieta, L.G. Bettini, El. Selli, Appl. Catal., B: Environ. 136/137 (2013) 81–88.
[8] L. Wei, Y.J. Chen, Y.P. Lin, H. Wu, R. Yuan, Z.H. Li, Appl. Catal., B: Environ. 144 (2014) 521–527.
[9] L. Wei, Y.J. Chen, Z.H. Li, Beilstein J. Nanotechnol. 4 (2013) 949–955.
[10] I. Tsuji, Y. Shimodaira, H. Kato, H. Kobayashi, A. Kudo, Chem. Mater. 22 (2010) 1402–1409.
[11] R. Sasaki, K. Maeda, Y. Kako, K. Domen, Appl. Catal., B: Environ. 128 (2012) 72–76.
[12] Z. Wang, J.G. Hou, C. Yang, S.Q. Jiao, K. Huang, H.M. Zhu, Energy Environ. Sci. 6 (2013) 2134–2144.
[13] X.C. Wang, K. Maeda, A. Thomas, K. Takanabe, G. Xin, J.M. Carlssom, K. Domen, M. Antonietti, Nat. Mater. 8 (2009) 76–82.
[14] Y.J. Chen, S. Hu, W. Liu, X. Chen, L. Wu, X. Wang, P. Liu, Z.H. Li, Dalton Trans. 40 (2011) 2607–2613.
[15] Y. Chen, R. Huang, D. Chen, Y. Wang, W. Liu, X. Li, Z.H. Li, Appl. Mater. Interfaces 4 (2012) 2273–2279.
[16] Z.B. Lei, W.S. You, M.Y. Liu, G.H. Zhou, T. Takata, M. Hara, K. Domen, C. Li, Chem. Commun. 17 (2003) 2142–2143.
[17] B. Chai, T.Y. Peng, P. Zeng, X. Zhang, X.J. Liu, J. Phys. Chem. C 115 (2011) 6149–6155.
[18] N.S. Chaudhari, A.P. Bhirud, R.S. Sonawane, L.K. Nikam, S.S. Warule, V.H. Rane, B.B. Kale, Green Chem. 13 (2011) 2500–2506.
[19] S. Shen, L. Zhao, Z. Zhou, L. Guo, J. Phys. Chem. C 112 (2008) 16148–116155.
[20] B. Chai, T. Peng, P. Zeng, X. Zhang, Dalton Trans. 41 (2012) 1179–1186.
[21] S. Peng, P. Zhu, S.G. Mhaisalkar, J. Phys. Chem. C 116 (2012) 13849–13857.
[22] J. Zhou, G. Tian, Y. Chen, X. Meng, Y. Shi, X. Cao, K. Pana, H. Fu, Chem. Commun. 49 (2013) 2237–2239.
[23] L. Ye, J.L. Fu, Z. Xu, R.S. Yuan, Z.H. Li, ACS Appl. Mater. Interfaces 6 (2014) 3483–3490.
[24] Y.J. Chen, H. Ge, L. Wei, Z.H. Li, R.S. Yuan, P. Liu, X.Z. Fu, Catal. Sci. Technol. 3 (2013) 1712–1717.
[25] Y. Hu, Y. Liu, H.S. Qian, Z.Q. Li, J.F. Chen, Langmuir 26 (2010) 18570–18575.
[26] M. Baghbanzadeh, L. Carbone, P.D. Cozzoli, C.O. Kappe, Angew. Chem. Int. Ed. 50 (2011) 2–50.
[27] W.M. Liu, M.Q. Shi, X.L. Lang, D. Zhao, Y.Q. Chu, C.A. Ma, Catal. Today 200 (2013) 87–93.
[28] B. Tryba, A.W. Morawski, M. Inagaki, Carbon 43 (2005) 2417–2419.
[29] E.H.L. Falcao, R.G. Blair, J.J. Mack, L.M. Viculis, C.W. Kwon, M. Bendikov, R.B. Kaner, B.S. Dunn, F. Wudl, Carbon 45 (2007) 1367–1369.
[30] Y. Liua, Y. Hu, M. Zhou, H.S. Qian, X. Hu, Appl. Catal., B: Environ. 125 (2012) 425–431.
[31] X.J. Liu, L.K. Pan, T. Lv, G. Zhu, Z. Suna, C.Q. Sunb, Chem. Commun. 47 (2011) 11984–11986.
[32] H.F. Li, H. Yu, S. Chen, H. Zhao, Y. Zhang, X. Quan, Dalton Trans. 43 (2014) 2888–2894.
[33] Y.W. Zhang, J.Q. Tian, H.Y. Li, L. Wang, X.Y. Qin, A.M. Asiri, A.O. Al-Youbi, X.P. Sun, Langmuir 28 (2012) 12893–12900.
[34] A. Iwase, Y.H. Ng, Y. Ishiguro, A. Kudo, R. Amal, J. Am. Chem. Soc. 133 (2011) 11054–11057.
[35] O. Akhavan, E. Ghaderi, J. Phys. Chem. C 113 (2009) 20214–20220.
[36] R. Huang, H. Ge, X. Lin, Y. Guo, R.S. Yuan, X.Z. Fu, Z.H. Li, RSC Adv. 3 (2013) 1235–1242.
[37] Y. Park, S.H. Kang, W.Y. Choi, Phys. Chem. Chem. Phys. 13 (2011) 9425–9431.
[38] Y. Liu, L. Zhou, Y. Hu, C.F. Guo, H.S. Qian, F.M. Zhang, X.W. Lou, J. Mater. Chem. 21 (2011) 18359–18364.
[39] S. Stankovich, D.A. Dikin, R.D. Piner, K.A. Kohlhaas, A. Kleinhammes, Y.Y. Jia, Y. Wu, Carbon 45 (2007) 1558–1565.
[40] L. Jia, D.H. Wang, Y.X. Huang, A.W. Xu, H.Q. Yu, J. Phys. Chem. C 115 (2011) 11466–11473.
[41] J.G. Yu, T.T. Ma, S.W. Liu, Phys. Chem. Chem. Phys. 13 (2011) 3491–3501.
[42] Q. Li, B.D. Guo, J.G. Yu, J.R. Ran, B.H. Zhang, H.J. Yan, J.R. Gong, J. Am. Chem. Soc. 133 (2011) 10878–10884.
[43] X.Y. Zhang, H.P. Li, X.L. Cui, Y.H. Lin, J. Mater. Chem. 20 (2010) 2801–2806.
[44] W.J. Yue, S.K. Han, R.X. Peng, W. Shen, H.W. Geng, F. Wu, S.W. Tao, M.T. Wang, J. Mater. Chem. 20 (2010) 7570–7578.